

# One-dimensional domain walls in thin ferromagnetic films with fourfold anisotropy

Ross G. Lund and Cyrill B. Muratov

Department of Mathematical Sciences, NJIT, University Heights, Newark, NJ 07102, USA

E-mail: [lund@njit.edu](mailto:lund@njit.edu), [muratov@njit.edu](mailto:muratov@njit.edu)

**Abstract.** We study the properties of domain walls and domain patterns in ultrathin epitaxial magnetic films with two orthogonal in-plane easy axes, which we call fourfold materials. In these materials, the magnetization vector is constrained to lie entirely in the film plane and has four preferred directions dictated by the easy axes. We prove the existence of  $90^\circ$  and  $180^\circ$  domain walls in these materials as minimizers of a nonlocal one-dimensional energy functional. Further, we investigate numerically the role of the considered domain wall solutions for pattern formation in a rectangular sample.

Mathematics Subject Classification: 78A30, 35Q60, 82D40

*Keywords:* magnetic domains, thin films, non-local variational problems

Submitted to: *Nonlinearity*

## 1. Introduction

Thin-film ferromagnetic materials have played a central role in information storage technologies for many years [1–3]. In this context, much attention has been devoted to studying these materials by both the physics and mathematics communities [1, 4]. Magnetic storage media make use of *magnetic domains*—regions of uniform magnetization separated by thin transition layers called *domain walls*—to represent bits of information. Typically, thin films possess one distinguished in-plane direction along which the magnetization prefers to align; this direction is referred to as an easy axis, and materials possessing a single easy axis as *uniaxial*. In such a material, this results in two distinct optimal domain orientations, which may be used to store binary information. More recently, more preference has been given to perpendicular materials — magnetic storage materials in which the easy axis is in the out-of-plane direction [2, 5]. Nevertheless, thin film materials with in-plane anisotropy continue to be important for many applications, such as magnetoresistive random access memory [6–10] and spintronics [11].

In this article, we study one-dimensional domain walls in thin ferromagnetic films in which the magnetization is strongly penalized from pointing out of the film plane, with two orthogonal in-plane easy axes (and thus four optimal magnetization directions). We refer to these materials as *ultrathin fourfold films*. Such behaviour is, for example, experimentally realized in very thin (3-19 monolayers thick) films of epitaxial cobalt and gives rise to unusual magnetic domain morphologies in which the magnetization vector has a tendency to rotate by integer multiples of  $90^\circ$  in the film plane [12, 13].

In order to understand the magnetization behaviour of thin-film materials from a theoretical point of view, one would like to study the formation of domain patterns, and the structure of the domain walls which connect them. We start from the Landau–Lifshitz–Gilbert (LLG) equation for the dynamics of the magnetization vector  $\mathbf{M}(\mathbf{x}, t)$ , which is of fixed length  $|\mathbf{M}(\mathbf{x}, t)| = M_s$  and defined on a spatial domain  $\Omega \subset \mathbb{R}^3$  representing the ferromagnetic body under study. The LLG equation for  $\mathbf{M}$  reads

$$\frac{\partial \mathbf{M}}{\partial t} = -\frac{\gamma}{1 + \alpha^2} (\mathbf{M} \times \mathbf{H} + \alpha \mathbf{M} \times \mathbf{M} \times \mathbf{H}), \quad \hat{\mathbf{n}} \cdot \nabla \mathbf{M}|_{\partial \Omega} = 0, \quad (1)$$

where  $\gamma$  is the gyromagnetic ratio,  $\alpha$  is the dimensionless Gilbert damping parameter, and  $\mathbf{H}$  is the effective magnetic field. This field is obtained via  $\mathbf{H} = -\delta E / \delta \mathbf{M}$ , where  $E(\mathbf{M})$  is the micromagnetic energy functional:

$$E(\mathbf{M}) = \frac{1}{2} \int_{\Omega} \left( \frac{A}{M_s^2} |\nabla \mathbf{M}|^2 + \frac{K}{M_s^2} \Phi(\mathbf{M}) - 2\mathbf{H}_a \cdot \mathbf{M} \right) d^3\mathbf{r} + \frac{1}{2} \int_{\mathbb{R}^3} \int_{\mathbb{R}^3} \frac{\nabla \cdot \mathbf{M}(\mathbf{r}) \nabla \cdot \mathbf{M}(\mathbf{r}')}{|\mathbf{r} - \mathbf{r}'|} d^3\mathbf{r} d^3\mathbf{r}'. \quad (2)$$

Here,  $A$  is the exchange constant;  $K$  is a crystalline anisotropy constant, with  $\Phi(\mathbf{M})$  a scalar function describing the anisotropy; and  $\mathbf{H}_a \in \mathbb{R}^3$  is an external applied magnetic field. The terms in the energy may be understood as follows. The first term is the exchange energy, which penalizes spatial variations of  $\mathbf{M}$ ; the second is the anisotropy energy, which describes the preferred directions for  $\mathbf{M}$  within a material; the third is the Zeeman energy, which prefers  $\mathbf{M}$  to align with the external field; and the fourth (in which  $\mathbf{M}$  is extended by zero outside of  $\Omega$  and the derivatives are understood in the distributional sense) is the nonlocal magnetostatic energy, which prefers to minimize the distributional divergence of  $\mathbf{M}$ . See e.g. [1] for further details of the micromagnetic model.

We can consider observable static domain patterns as stationary (i.e. with  $\frac{\partial \mathbf{M}}{\partial t} = 0$ ) solutions of (1), and note that, in this case, equation (1) coincides with the Euler–Lagrange equation for  $E$  incorporating the pointwise constraint  $|\mathbf{M}| = M_s$ . This will enable us to employ variational techniques to characterize solutions.

We consider a reduction of the micromagnetic theory appropriate for very thin films. Many such reductions have been presented before [14–18], corresponding to a variety of regimes of the physical parameters in the energy (2). In order to understand

the parameter regime we study here, we introduce the following quantities:

$$\ell = \left( \frac{A}{4\pi M_s^2} \right)^{1/2}, \quad L = \left( \frac{A}{K} \right)^{1/2}, \quad Q = \left( \frac{\ell}{L} \right)^2, \quad (3)$$

respectively called the exchange length, Bloch wall width, and quality factor. In extended films, we may take the spatial domain  $\Omega = \mathbb{R}^2 \times (0, d)$ , where  $d$  is the film thickness. The physical regime we consider is then characterized by the scalings  $d \lesssim \ell \lesssim L$ , with  $Ld/\ell^2 \sim 1$ . This regime (ultrathin, moderately soft film) is relevant for a variety of materials [19]. In this regime, one may introduce the dimensionless *thin-film parameter*

$$\nu = \frac{4\pi M_s^2 d}{KL} = \frac{Ld}{\ell^2} = \frac{d}{\ell\sqrt{Q}}, \quad (4)$$

which characterizes the strength of the magnetostatic interaction relative to both exchange and anisotropy.

One may then formally derive a reduced LLG equation from (1) by considering the limit  $Q \rightarrow 0$  and  $d \rightarrow 0$  together with  $\nu = O(1)$  fixed [20, 21]. Letting  $\mathbf{m} = \mathbf{M}/M_s$  and assuming  $\mathbf{m} = (m_1, m_2, 0)$ , i.e., that  $\mathbf{m}$  lies entirely within the film plane, after suitable rescalings one finds the effective overdamped equation

$$\frac{\partial \mathbf{m}}{\partial t} = -\mathbf{m} \times \mathbf{m} \times \mathbf{h}. \quad (5)$$

Here,  $\mathbf{h}$  is the effective field obtained now as  $\mathbf{h} = -\delta\mathcal{E}/\delta\mathbf{m}$ , where  $\mathcal{E}$  is the reduced thin-film energy

$$\mathcal{E}(\mathbf{m}) = \frac{1}{2} \int_{\mathbb{R}^2} (|\nabla \mathbf{m}|^2 + \Phi(\mathbf{m})) \, d^2\mathbf{r} + \frac{\nu}{8\pi} \int_{\mathbb{R}^2} \int_{\mathbb{R}^2} \frac{\nabla \cdot \mathbf{m}(\mathbf{r}) \nabla \cdot \mathbf{m}(\mathbf{r}')}{|\mathbf{r} - \mathbf{r}'|} \, d^2\mathbf{r} \, d^2\mathbf{r}', \quad (6)$$

and now  $\mathbf{m} : \mathbb{R}^2 \rightarrow \mathbb{S}^1$  is the in-plane magnetization direction field. In what follows, we consider the case of

$$\Phi(\mathbf{m}) = (\mathbf{m} \cdot \mathbf{e}_1)^2 (\mathbf{m} \cdot \mathbf{e}_2)^2, \quad (7)$$

corresponding to fourfold anisotropy. This type of magnetocrystalline anisotropy is very common for ultrathin epitaxial films [19]. Ultrathin films with this type of anisotropy has been proposed for applications to multi-level magnetoresistive random access memories [22, 23] and could be of interest to domain wall based devices [10, 24].

In uniaxial thin films, the behaviour of  $180^\circ$  domain walls has been extensively studied. For simple one-dimensional profiles connecting the two optimal directions, there are two possibilities: the *Bloch wall*, in which the magnetization transitions between the optimal domains by rotating out of the film plane, and the *Néel wall*, in which the rotation occurs entirely within the plane. Which wall type is energetically preferred depends essentially on how severe the penalty for rotating out of plane is, which in turn depends on the film thickness. In the ultrathin regime we consider in this article, this penalty is strong enough to simply forbid any out of plane component of  $\mathbf{m}$ , so that the Néel wall profile is the only choice.

Néel walls have been studied for many years, with a degree of controversy (see e.g. [1,25]). More recent micromagnetic studies have led to a good present understanding of the Néel wall's internal structure [1,4,26–31], the main features of which (sharp inner core with slowly decaying tails) have been verified experimentally [32–34].

Rigorous mathematical studies of the Néel walls began with the work of GARCIA-CERVERA, who studied, both analytically and numerically, the one-dimensional variational problem obtained from the full micromagnetic energy by restricting to profiles which depend only on one spatial variable [26,27]. The same functional was studied by MELCHER, who restricted the admissible magnetization configurations to those constrained to the film plane, and established symmetry and monotonicity of minimizers connecting the two optimal directions [28]. Uniqueness of the Néel wall profile and its linearized stability with respect to one-dimensional perturbations was treated by CAPELLA, OTTO AND MELCHER [29]. Stability of geometrically constrained Néel walls with respect to large two-dimensional perturbations has been demonstrated asymptotically in [35]. Most recently a comprehensive study of Néel walls under the influence of applied magnetic fields was undertaken by CHERMISI AND MURATOV [30]. They proved existence, uniqueness, strict monotonicity and smoothness of the wall profile along with estimates for its asymptotic decay.

To summarize, in ultrathin uniaxial films the magnetization is effectively constrained to lie completely in the film plane, and one encounters  $180^\circ$  Néel walls as the optimal transition layer profiles connecting the two uniform states. These are now well understood. Beyond that, it is possible to observe stable *winding domain walls*, in which the magnetization makes a number of full  $360^\circ$  rotations (most often just one, though more are possible) [36–38]. This type of domain walls has received recent theoretical attention in [39,40]. A reproducible way to inject  $360^\circ$  walls into ferromagnetic nanowires and successful manipulation of such domain walls were recently demonstrated experimentally in [41,42].

In fourfold films with in-plane magnetizations, we can make the following analogies with the uniaxial case. In fourfold materials, the  $90^\circ$ -walls are expected to exist as optimal profiles connecting two adjacent minima of the potential  $\Phi$  (e.g.  $+\mathbf{e}_1$  and  $+\mathbf{e}_2$ ). This is analogous to the  $180^\circ$  Néel walls in uniaxial materials. For a  $180^\circ$ -wall in a fourfold material, the magnetization has to connect two nonadjacent minima of  $\Phi$  while passing directly through a third somewhere in between (i.e. connect  $+\mathbf{e}_1$  and  $-\mathbf{e}_1$ , while passing through  $+\mathbf{e}_2$ ). Moreover, this should occur without the wall simply splitting into two separate  $90^\circ$ -walls. This is analogous to the  $360^\circ$ -walls in uniaxial materials.

In this article we extend the methods contained in previous work concerning  $180^\circ$  and  $360^\circ$  domain walls in uniaxial materials to the setting of fourfold materials, and prove existence results for both  $90^\circ$  and  $180^\circ$  walls in these materials. These walls, despite some apparent analogies with those found in uniaxial films, have not been previously investigated theoretically.

### 1.1. Reduced model for one-dimensional domain walls

Since stationary solutions of (5) coincide with critical points of (6), in order to study stationary one-dimensional domain wall profiles, we now seek to derive a 1D variational problem from (6) which is appropriate to capture such profiles via minimization.

In what follows we explicitly restrict to stationary profiles,  $\mathbf{m}(x_1, x_2, t) = \mathbf{m}(x_1, x_2)$ . It is convenient to introduce the in-plane magnetization angle  $\theta : \mathbb{R}^2 \rightarrow \mathbb{R}$  via

$$\mathbf{m} = -\mathbf{e}_1 \sin \theta + \mathbf{e}_2 \cos \theta. \quad (8)$$

We now assume a one-dimensional profile  $\theta(x_1, x_2) = \theta(\xi)$  varying only along the direction  $\mathbf{e}_\xi = \mathbf{e}_1 \cos \beta + \mathbf{e}_2 \sin \beta$ ; we refer to the angle  $\beta$  as the *wall orientation*. With these assumptions, the LLG equation (5) for a stationary 1D profile  $\theta(x)$  reduces to

$$0 = -\theta_{xx} + \frac{1}{4} \sin 4\theta + \frac{\nu}{2} \cos(\theta - \beta) \left( -\frac{d^2}{dx^2} \right)^{1/2} \sin(\theta - \beta), \quad (9)$$

where  $\left( -\frac{d^2}{dx^2} \right)^{1/2}$  is the negative 1D half-Laplacian (a linear operator from  $H^1(\mathbb{R})$ , modulo additive constants, to  $L^2(\mathbb{R})$  whose Fourier symbol is  $|k|$ ). Equation (9) is also the Euler–Lagrange equation corresponding to the energy

$$\mathcal{E}_\beta(\theta) = \frac{1}{2} \int_{\mathbb{R}} \left( |\theta'|^2 + \frac{1}{4} \sin^2 2\theta \right) dx + \frac{\nu}{4} \|\sin(\theta - \beta)\|_{H^{1/2}(\mathbb{R})}^2, \quad (10)$$

where we introduced the homogeneous  $H^{1/2}(\mathbb{R})$  (semi-)norm [43]:

$$\|u\|_{H^{1/2}(\mathbb{R})}^2 = \int_{\mathbb{R}} u \left( -\frac{d^2}{dx^2} \right)^{1/2} u dx = \frac{1}{2\pi} \int_{\mathbb{R}} \int_{\mathbb{R}} \frac{(u(x) - u(y))^2}{(x - y)^2} dx dy. \quad (11)$$

It is not too difficult to see that this energy corresponds to the energy (6) of a 1D profile per unit width in the transverse direction.

This model forms the basis of the rest of this article. It is necessary to specialize it further to individually examine the two types of wall we study:  $90^\circ$  and  $180^\circ$  walls. To state our main results, we need to introduce the following general admissible class of functions for a given  $\alpha \in \mathbb{R}$ :

$$\mathcal{A}_\alpha = \{\theta \in H_{\text{loc}}^1(\mathbb{R}) : \theta - \eta_\alpha \in H^1(\mathbb{R})\},$$

where  $\eta_\alpha \in C^\infty(\mathbb{R})$  is a fixed function which satisfies

$$\eta_\alpha(x) = \begin{cases} \alpha & \text{for } x \in (-\infty, -1), \\ 0 & \text{for } x \in (1, +\infty). \end{cases}$$

It is easy to see that the definition of the admissible class  $\mathcal{A}_\alpha$  does not depend on the specific choice of  $\eta_\alpha$  [30]. Also, by Morrey's theorem we may always assume that if  $\theta \in \mathcal{A}_\alpha$ , then  $\theta \in C(\mathbb{R}) \cap L^\infty(\mathbb{R})$  and that  $\lim_{x \rightarrow +\infty} \theta(x) = 0$  and  $\lim_{x \rightarrow -\infty} \theta(x) = \alpha$ .

In the following, we will look for minimizers of the one-dimensional domain wall energy  $\mathcal{E}_\beta$  in the admissible classes  $\mathcal{A}_\alpha$  with  $\alpha = \pi/2$  and  $\alpha = \pi$  to study  $90^\circ$  and  $180^\circ$  walls, respectively.

## 2. Main Results

We are now in a position to state the main results of this work. The first result below concerns 90°-walls, and provides existence of these as energy minimizing configurations. These profiles only exist for a particular orientation  $\beta = -\pi/4$  (modulo  $\pi/2$  rotations). Furthermore, we are able to extract further information on the profiles including uniqueness, smoothness, and strict monotonicity.

**Theorem 1** (90°-walls: existence, uniqueness, regularity and strict monotonicity). *For  $\beta = -\pi/4$  and each  $\nu > 0$ , there exists a minimizer of the energy  $\mathcal{E}_\beta(\theta)$  over the admissible class  $\mathcal{A}_{\pi/2}$ . The minimizer is unique (up to translations), strictly decreasing with range equal to  $(0, \pi/2)$ , and is a smooth solution of (9) satisfying the limit conditions*

$$\lim_{x \rightarrow +\infty} \theta(x) = 0, \quad \lim_{x \rightarrow -\infty} \theta(x) = \pi/2. \quad (12)$$

Moreover, if  $\theta^{(0)} : \mathbb{R} \rightarrow (0, \pi/2)$  is the minimizer of  $\mathcal{E}_{-\pi/4}(\theta)$  over  $\mathcal{A}_{\pi/2}$  satisfying  $\theta^{(0)}(0) = \pi/4$ , then  $\theta^{(0)}(x) = \pi/2 - \theta^{(0)}(-x)$ .

The choice of the admissible class  $\mathcal{A}_{\pi/2}$  serves to enforce the asymptotic behavior in (12). We note that for other wall orientations  $\beta$  the wall would carry a net line “charge” and, hence, the last term in the one-dimensional wall energy (10) would always be infinite on  $\mathcal{A}_{\pi/2}$ .

The next result is similar to the first, but concerning 180°-walls. Again the orientation of the walls is restricted, this time to  $\beta = 0$  (modulo  $\pi/2$  rotations). Many of the properties of 90° walls follow here, though uniqueness of the profile is not presently clear.

**Theorem 2** (180°-walls: existence, regularity and strict monotonicity). *For  $\beta = 0$  and each  $\nu > 0$ , there exists a minimizer of the energy  $\mathcal{E}_\beta(\theta)$  over the admissible class  $\mathcal{A}_\pi$ . The minimizer is strictly decreasing with range equal to  $(0, \pi)$ , and is a smooth solution of (9) satisfying the limit conditions*

$$\lim_{x \rightarrow +\infty} \theta(x) = 0, \quad \lim_{x \rightarrow -\infty} \theta(x) = \pi. \quad (13)$$

Moreover, if  $\theta^{(0)} : \mathbb{R} \rightarrow (0, \pi)$  is the minimizer of  $\mathcal{E}_0(\theta)$  over  $\mathcal{A}_\pi$  satisfying  $\theta^{(0)}(0) = \pi/2$ , then  $\theta^{(0)}(x) = \pi - \theta^{(0)}(-x)$ .

Similarly to the case of 90°-walls, the choice of the admissible class  $\mathcal{A}_\pi$  ensures the conditions (13) at infinity, and for other choices of wall orientation there is a net line charge as well.

The remainder of this article is structured as follows. In §3, we present proofs of the results given above, using primarily variational methods. In §4, we conduct a numerical study of 1D domain walls in fourfold materials using 1D simulations, and perform 2D simulations of a rectangular film element to observe static magnetization configurations involving these walls. Finally in §5 we conclude and suggest some further extensions to this work.

### 3. Proofs of main results

The following section is devoted to motivating the statements of theorems 1 and 2, and presenting their proofs.

#### 3.1. 90° walls: Proof of theorem 1

Let us begin by motivating the precise statement of the theorem. Firstly we note that in principle, the result one would like to obtain is existence of a solution to (9) which satisfies (without loss of generality) the conditions

$$\lim_{x \rightarrow +\infty} \theta(x) = 0, \quad \lim_{x \rightarrow -\infty} \theta(x) = \pi/2, \quad (14)$$

and is in some sense physical, i.e. having finite energy per unit length of the domain wall. Let us recall the energy per unit length in (10) for a 1D wall of orientation  $\beta$ . In explicit terms, it reads

$$\begin{aligned} \mathcal{E}_\beta(\theta) = & \frac{1}{2} \int_{\mathbb{R}} \left( |\theta'|^2 + \frac{1}{4} \sin^2 2\theta \right) dx \\ & + \frac{\nu}{8\pi} \int_{\mathbb{R}} \int_{\mathbb{R}} \frac{(\sin(\theta(x) - \beta) - \sin(\theta(y) - \beta))^2}{(x - y)^2} dx dy. \end{aligned} \quad (15)$$

We would like to choose an admissible class of minimizers corresponding to 90° transition layers with finite energy which connect two of the global minima of  $\mathcal{E}_\beta$  (given by  $\theta(x) = N\pi/2$  for any  $N \in \mathbb{Z}$ ). Without loss of generality, we can consider profiles satisfying (14). For  $\theta \in H_{\text{loc}}^1(\mathbb{R})$  the local part of the energy is locally well-defined. In order that the nonlocal term be finite for such profiles, we must constrain the wall orientation  $\beta$  appropriately so as to avoid incurring a net magnetic charge across the wall. To accomplish this we take  $\beta = -\pi/4$ .

The 1D 90°-wall energy may be expressed as

$$\mathcal{E}_{-\pi/4}(\theta) = \frac{1}{2} \int_{\mathbb{R}} \left( |\theta'|^2 + \frac{1}{4} \sin^2 2\theta \right) dx + \frac{\nu}{4} \|\sin(\theta + \pi/4)\|_{\dot{H}^{1/2}(\mathbb{R})}^2, \quad (16)$$

and the Euler–Lagrange equation associated to  $\mathcal{E}_{-\pi/4}$  is now given formally by

$$0 = -\theta_{xx} + \frac{1}{4} \sin 4\theta + \frac{\nu}{2} \cos(\theta + \pi/4) \left( -\frac{d^2}{dx^2} \right)^{1/2} \sin(\theta + \pi/4), \quad (17)$$

with limit conditions (14).

The motivation for the statement of theorem 1 should now be clear. We present a slightly abbreviated proof of this result; much of the machinery follows directly from the work of CHERMISI AND MURATOV [30] concerning Néel walls in uniaxial materials. Thus we refer the reader to their work when proving certain steps, and focus here on aspects which are significantly different.

It is convenient to first record some preliminary lemmas.



**Lemma 1** (Restriction of rotations). *Let  $\theta \in \mathcal{A}_{\pi/2}$ . Then there exists  $\tilde{\theta} \in \mathcal{A}_{\pi/2}$  such that  $\tilde{\theta}(\mathbb{R}) \subset [0, \pi/2]$  and  $\mathcal{E}_{-\pi/4}(\tilde{\theta}) \leq \mathcal{E}_{-\pi/4}(\theta)$ .*

*Proof.* We let  $\theta^T : \mathbb{R} \rightarrow [0, \pi/2]$  be defined, for  $k \in \mathbb{Z}$ , by

$$\theta^T(x) = \begin{cases} \theta(x) - k\pi & \text{if } \theta(x) \in [k\pi, (k + \frac{1}{2})\pi), \\ k\pi - \theta(x) & \text{if } \theta(x) \in [(k - \frac{1}{2})\pi, k\pi). \end{cases}$$

We then have

$$\|\sin 2\theta\|_{L^2(\mathbb{R})}^2 = \|\sin 2\theta^T\|_{L^2(\mathbb{R})}^2, \quad \|\theta'\|_{L^2(\mathbb{R})}^2 = \|(\theta^T)'\|_{L^2(\mathbb{R})}^2,$$

and the inequality in the lemma follows from setting  $\tilde{\theta} = \theta^T$ , the inequality

$$\|u\|_{\dot{H}^{1/2}}^2 = \int_{\mathbb{R}} u \left( -\frac{d^2}{dx^2} \right)^{1/2} u \, dx \geq \int_{\mathbb{R}} |u| \left( -\frac{d^2}{dx^2} \right)^{1/2} |u| \, dx,$$

and the fact that  $|\sin(\theta + \pi/4)| = \sin(\theta^T + \pi/4)$ .  $\square$

Given this lemma, we may restrict the admissible class to those  $\theta \in \mathcal{A}_{\pi/2}$  also satisfying  $\theta(\mathbb{R}) \subset [0, \pi/2]$ . It is then useful to define a function  $\rho : \mathbb{R} \rightarrow [0, \pi/4] \in H^1(\mathbb{R})$ , corresponding to each  $\theta$  in this restricted class, via

$$\rho(x) = \begin{cases} \theta(x) & \text{if } \theta(x) \in [0, \pi/4], \\ \pi/2 - \theta(x) & \text{if } \theta(x) \in [\pi/4, \pi/2]. \end{cases} \quad (18)$$

It is clear that  $\rho$  satisfies  $\mathcal{E}_{-\pi/4}(\rho) = \mathcal{E}_{-\pi/4}(\theta)$ . One then has the following lemma:

**Lemma 2** (Coercivity). *Let  $\theta \in \mathcal{A}_{\pi/2}$  be such that  $\theta(\mathbb{R}) \subset [0, \pi/2]$  and let  $\rho$  be defined as in (18). Then*

$$\mathcal{E}_{-\pi/4}(\rho) \geq \frac{1}{4} \|\rho\|_{H^1(\mathbb{R})}^2 + \frac{\nu}{4} \|\sin(\rho + \pi/4)\|_{\dot{H}^{1/2}(\mathbb{R})}^2.$$

*Proof.* The bound follows immediately from the fact that, since  $\rho(x) \in [0, \pi/4]$  for all  $x \in \mathbb{R}$ , one has

$$\cos \rho(x) \geq 1/\sqrt{2}, \quad \sin \rho(x) \geq \rho(x)/\sqrt{2},$$

and the identity  $\sin^2 2\rho = 4 \sin^2 \rho \cos^2 \rho$ .  $\square$

The following lemma provides useful properties for candidate minimizers.

**Lemma 3** (Rearrangement). *Let  $\theta \in \mathcal{A}_{\pi/2}$  with  $\theta(\mathbb{R}) \subset [0, \pi/2]$ . Then  $\exists \theta^o \in C(\mathbb{R}; [0, \pi/2])$  satisfying  $\mathcal{E}_{-\pi/4}(\theta^o) \leq \mathcal{E}_{-\pi/4}(\theta)$  and the following properties:*

$$\lim_{x \rightarrow +\infty} \theta^o(x) = 0, \quad \lim_{x \rightarrow -\infty} \theta^o(x) = \frac{\pi}{2}, \quad \theta^o(0) = \frac{\pi}{4}, \quad \theta^o(x) = \frac{\pi}{2} - \theta^o(-x),$$

and  $\theta^o$  is non-increasing.



*Proof.* The proof here is similar to that of lemma 4 in [30]. Let  $\rho : \mathbb{R} \rightarrow [0, \pi/4]$  be defined as in (18) and let  $\rho^*$  denote its symmetric decreasing rearrangement. By standard properties of rearrangements (as in [30]) we have firstly that

$$\int_{\mathbb{R}} \sin^2 2\rho^* dx = \int_{\mathbb{R}} \sin^2 2\rho dx. \quad (19)$$

Secondly,

$$[\sin(\rho + \pi/4) - \sin(\pi/4)]^* = \sin(\rho^* + \pi/4) - \sin(\pi/4).$$

Using this, along with lemma 3 in [30], we see that

$$\|\sin(\rho + \frac{\pi}{4})\|_{\dot{H}^{1/2}(\mathbb{R})}^2 \geq \|\sin(\rho^* + \frac{\pi}{4})\|_{\dot{H}^{1/2}(\mathbb{R})}^2. \quad (20)$$

From [43, Lemma 7.17], we have

$$\int_{\mathbb{R}} (\rho_x^*)^2 dx \leq \int_{\mathbb{R}} \rho_x^2 dx. \quad (21)$$

Thus, combining (19), (20), and (21), we obtain

$$\mathcal{E}_{-\pi/4}(\rho^*) \leq \mathcal{E}_{-\pi/4}(\rho) = \mathcal{E}_{-\pi/4}(\theta).$$

Finally, defining  $\theta^o \in C(\mathbb{R}; [0, \pi/2])$  via

$$\theta^o(x) = \begin{cases} \rho^*(x) & \text{if } x \geq 0 \\ \pi/2 - \rho^*(-x) & \text{if } x < 0, \end{cases} \quad (22)$$

it is clear that  $\mathcal{E}_{-\pi/4}(\theta^o) = \mathcal{E}_{-\pi/4}(\rho^*)$ , and that  $\theta^o$  satisfies the properties given in the lemma.  $\square$

We now turn to the proof of theorem 1.

*Step 1: Existence.* Take a minimizing sequence  $\{\theta_n\} \subset \mathcal{A}_{\pi/2}$ . By translation-invariance and lemmas 1 and 3 we may assume

$$\theta_n \in C(\mathbb{R}; [0, \pi/2]), \quad \theta_n(0) = \pi/4, \quad \theta_n(x) = \pi/2 - \theta_n(-x),$$

and  $\theta_n$  are non-increasing. For each  $n$ , define  $\rho_n : \mathbb{R} \rightarrow [0, \pi/4]$  as in (18). From lemma 2 we have

$$\frac{1}{4} \|\rho_n\|_{H^1(\mathbb{R})}^2 + \frac{\nu}{4} \|u_n\|_{\dot{H}^{1/2}(\mathbb{R})}^2 \leq C < \infty,$$

where  $u_n = \sin(\rho_n + \pi/4) - \sin(\pi/4)$ . We may then extract a subsequence (not relabelled) such that the following weak convergences hold:

$$\rho_n \rightharpoonup \rho \text{ in } H^1(\mathbb{R}), \quad u_n \rightharpoonup u \text{ in } H^{1/2}(\mathbb{R}),$$

Moreover, by compact embedding of the spaces  $H^1(\mathbb{R})$  and  $H^{1/2}(\mathbb{R})$  into  $L_{loc}^2(\mathbb{R})$ , we have, upon extraction of a further subsequence:

$$\rho_n \rightarrow \rho \text{ and } u_n \rightarrow u \text{ strongly in } L_{loc}^2(\mathbb{R}) \text{ and a.e. in } \mathbb{R}.$$

Therefore, we have  $u = \sin(\rho + \pi/4) - \sin(\pi/4)$  a.e. in  $\mathbb{R}$ . Then, using Fatou's lemma applied to the second term in the definition of the energy and lower semicontinuity of homogeneous  $H^1(\mathbb{R})$  and  $H^{1/2}(\mathbb{R})$  norms, one obtains weak lower semicontinuity of  $\mathcal{E}_{-\pi/4}(\rho)$  with respect to the weak convergences considered. Passing to the limit  $n \rightarrow \infty$ , we thus obtain

$$\mathcal{E}_{-\pi/4}(\rho) \leq \liminf_{n \rightarrow \infty} \mathcal{E}_{-\pi/4}(\rho_n) = \liminf_{n \rightarrow \infty} \mathcal{E}_{-\pi/4}(\theta_n).$$

Given such a  $\rho$ , we construct a function  $\theta^{(0)} : \mathbb{R} \rightarrow [0, \pi/2]$  as in (22), that has the properties

$$\theta^{(0)}(0) = \pi/4, \quad \theta^{(0)}(x) = \pi/2 - \theta^{(0)}(-x), \quad \lim_{x \rightarrow +\infty} \theta^{(0)}(x) = 0,$$

and  $\theta^{(0)}$  is non-increasing. Since  $\mathcal{E}_{-\pi/4}(\rho) = \mathcal{E}_{-\pi/4}(\theta^{(0)})$ , we then conclude that  $\theta^{(0)}$  is a minimizer.

*Step 2: Regularity.* Since  $\theta^{(0)}$  is a minimizer, it must also be a weak solution to (17). That is,  $\psi = \theta^{(0)}$  is a weak solution of the equation

$$\psi'' + a(x) \cos 2\psi + b(x) \cos(\psi + \pi/4) = 0, \quad (23)$$

where  $a(x) = \frac{1}{2} \sin 2\theta^{(0)}$  and  $b(x) = \frac{\nu}{2} \left(-\frac{d^2}{dx^2}\right)^{1/2} \sin(\theta + \pi/4)$ . It is easy to see from monotonicity of  $\theta^{(0)}(x)$  and the limit conditions (14) that  $a(x) \in L^2(\mathbb{R})$ . Moreover, since

$$\left\| \left(-\frac{d^2}{dx^2}\right)^{1/2} u \right\|_{L^2(\mathbb{R})}^2 = \left\| \frac{du}{dx} \right\|_{L^2(\mathbb{R})}^2 \quad \forall u \in H^1(\mathbb{R}), \quad (24)$$

and since  $[\sin(\theta^{(0)} + \pi/4)]' \in L^2(\mathbb{R})$ , we may see that  $b(x) \in L^2(\mathbb{R})$ , as well. Examining (23), we may then conclude that  $\theta_{xx}^{(0)} \in L^2(\mathbb{R})$ , and thus that  $\theta_x^{(0)} \in H^1(\mathbb{R})$ . Furthermore, Morrey's theorem then tells us that  $\theta_x^{(0)} \in C(\mathbb{R}) \cap L^\infty(\mathbb{R})$ , and so  $\theta^{(0)} \in C^1(\mathbb{R})$ . Going a step further, we differentiate  $a(x)$  and  $b(x)$  to get  $a'(x) = \sin 2\theta^{(0)} \cos 2\theta^{(0)} \theta_x^{(0)}$  and  $b'(x) = \frac{\nu}{2} \left(-\frac{d^2}{dx^2}\right)^{1/2} [(\sin(\theta^{(0)} + \pi/4))_x]$ . Clearly  $a'(x) \in L^2(\mathbb{R})$ , so  $a \in H^1(\mathbb{R})$ .

We would like to show the same for  $b(x)$ . Applying (24) to  $u = (\sin(\theta^{(0)} + \pi/4))_x$ , this then amounts to having to show that  $u_x \in L^2(\mathbb{R})$  (we already know that  $u \in L^2(\mathbb{R})$ ). We have  $u_x = (\sin(\theta^{(0)} + \pi/4))_{xx} = \theta_{xx}^{(0)} \cos(\theta^{(0)} + \pi/4) - (\theta_x^{(0)})^2 \sin(\theta^{(0)} + \pi/4)$ . Applying the interpolation inequality as in [29]:

$$\|\theta_x^{(0)}\|_{L^4(\mathbb{R})} \leq \|\theta_x^{(0)}\|_{L^\infty(\mathbb{R})}^{1/2} \|\theta_x^{(0)}\|_{L^2(\mathbb{R})}^{1/2} < \infty,$$

one may then conclude that  $b'(x) \in L^2(\mathbb{R})$ . Again, from (23), this gives  $\theta_{xx}^{(0)} \in H^1(\mathbb{R})$  and thus  $\theta_{xx}^{(0)} \in C(\mathbb{R}) \cap L^\infty(\mathbb{R})$ , implying that  $\theta^{(0)} \in C^2(\mathbb{R})$  is a classical solution to (17). These arguments may then be bootstrapped to conclude that  $\theta^{(0)} \in C^\infty(\mathbb{R})$ .

*Step 3: Strict monotonicity.* The proof here is similar to that in [30]. From the previous steps we know that  $\theta_x^{(0)} \leq 0$  on  $\mathbb{R}$  and  $\theta^{(0)} \in C^\infty(\mathbb{R})$ . We claim that in fact  $\theta_x^{(0)} < 0$  on  $\mathbb{R}$ . First, as in [29], we show  $\theta_x^{(0)}(0) < 0$ : if we assume  $\theta^{(0)}(0) = \pi/4$

and  $\theta_x^{(0)}(0) = 0$ , then uniqueness of solutions for the initial value problem implies  $\theta^{(0)}(x) = \pi/4$  identically, contradicting the limit conditions (14).

Next, we show  $\theta_x^{(0)} < 0$  on  $\mathbb{R}^+$ . Assume there exists an  $x_* > 0$  such that this is false: i.e.  $\theta_x^{(0)}(x_*) = 0$ . This, together with the non-increasing property of  $\theta^{(0)}(x)$  we already have, implies that  $\theta_{xx}^{(0)}(x_*) = 0$  as well. Differentiating the Euler–Lagrange equation and evaluating at  $x_*$ , we then have

$$\theta_{xxx}^{(0)}(x_*) = \frac{\nu}{2} \cos(\theta^{(0)}(x_*) + \pi/4) g(x_*),$$

where we defined

$$g(x) = \left( -\frac{d^2}{dx^2} \right)^{1/2} \cos(\theta^{(0)}(x) + \pi/4).$$

Computing  $g(x_*)$  directly, using the integral representation of  $\left( -\frac{d^2}{dx^2} \right)^{1/2}$  and noticing that by the assumption on  $x_*$  the obtained integral converges, we find

$$g(x) = -\frac{1}{\pi} \int_0^\infty \frac{4x_* y \theta_x^{(0)}(y) \cos(\theta^{(0)}(y) + \pi/4)}{(x_* - y)^2 (x_* + y)^2} dy.$$

Since  $\theta_x^{(0)} \leq 0$  on  $\mathbb{R}$ , with the inequality strict on a set of positive measure, we see that  $g(x_*) > 0$ . Moreover, we know that  $\cos(\theta^{(0)} + \pi/4) > 0$  on  $\mathbb{R}^+$ , and hence  $\theta_{xxx}^{(0)}(x_*) > 0$ , implying that  $\theta^{(0)}$  is locally increasing at  $x_*$ . This is a contradiction. Strict monotonicity on  $\mathbb{R}$  follows from the fact that  $\theta^{(0)}(x) = \pi/2 - \theta^{(0)}(-x)$  as proved in step 1.

*Step 4: Uniqueness (up to translations).* Let  $\theta^{(1)}$  and  $\theta^{(2)}$  be two distinct minimizers. After suitable translations these satisfy  $\theta^{(1)}(0) = \theta^{(2)}(0) = \pi/4$ . Define  $u = \sin(\theta + \pi/4)$ . We may write the energy  $\mathcal{E}_{-\pi/4}$  in terms of  $u$  as  $\mathcal{E}_{-\pi/4}(\theta) = E(u)$ , where

$$E(u) = \frac{1}{2} \int_{\mathbb{R}} \frac{u_x^2}{1 - u^2} dx + \frac{1}{2} \int_{\mathbb{R}} \left( u^2 - \frac{1}{2} \right)^2 dx + \frac{\nu}{4} \int_{\mathbb{R}} u \left( -\frac{d^2}{dx^2} \right)^{1/2} u dx$$

Then define

$$\tilde{\theta}(x) = \begin{cases} \sin^{-1}(\frac{1}{2}(u^{(1)}(x) + u^{(2)}(x))) - \pi/4 & \text{if } x \geq 0, \\ 3\pi/4 - \sin^{-1}(\frac{1}{2}(u^{(1)}(x) + u^{(2)}(x))) & \text{if } x < 0, \end{cases}$$

where  $u^{(1)} = \sin(\theta^{(1)} + \pi/4)$  and  $u^{(2)} = \sin(\theta^{(2)} + \pi/4)$ . Note that  $\sin(\tilde{\theta} + \pi/4) = \frac{1}{2}(u^{(1)} + u^{(2)})$ , and is symmetric decreasing.

Arguing as in [30], we have

$$(\tilde{\theta}_x)^2 \leq \frac{(\theta_x^{(1)})^2 + (\theta_x^{(2)})^2}{2}.$$

Then, since the last two terms in  $E(u)$  above are strictly convex in  $u$  (at least, for  $u \in [\frac{1}{\sqrt{2}}, 1]$ , which is equal to the possible range of values of  $u$  that we have here), we have that

$$\mathcal{E}_{-\pi/4}(\tilde{\theta}) < \frac{\mathcal{E}_{-\pi/4}(\theta^{(1)}) + \mathcal{E}_{-\pi/4}(\theta^{(2)})}{2},$$

which contradicts the minimality of  $\theta^{(1)}$  and  $\theta^{(2)}$ . This concludes the proof of Theorem 1.

**Remark 1.** *It should be possible to use the arguments of [31] to prove that the minimizers in theorem 1 are the unique monotone  $90^\circ$  wall profiles, i.e., that the minimizers are the unique, up to translations, monotone critical points of the energy  $\mathcal{E}_{-\pi/4}$  in  $\mathcal{A}_{\pi/2}$ .*

### 3.2. $180^\circ$ walls: Proof of theorem 2

Similarly to the above analysis of  $90^\circ$ -walls, we would first like to write down a 1D wall energy for  $180^\circ$ -walls and define an appropriate admissible class for minimizers. We assume, without loss of generality, a profile connecting the optimal uniform states  $\theta = \pi$  at  $-\infty$  and  $\theta = 0$  at  $+\infty$ . The appropriate wall orientation to avoid net charge is given by  $\beta = 0$ . The 1D wall energy is thus expressed as

$$\mathcal{E}_0(\theta) = \frac{1}{2} \int_{\mathbb{R}} \left( |\theta'|^2 + \frac{1}{4} \sin^2 2\theta \right) dx + \frac{\nu}{4} \|\sin \theta\|_{H^{1/2}(\mathbb{R})}^2, \quad (25)$$

with the admissible class for minimizers given by  $\mathcal{A}_\pi$ . The Euler–Lagrange equation associated to  $\mathcal{E}_0$  is given by

$$0 = -\theta_{xx} + \frac{1}{4} \sin 4\theta + \frac{\nu}{2} \cos \theta \left( -\frac{d^2}{dx^2} \right)^{1/2} \sin \theta, \quad (26)$$

with limit conditions

$$\lim_{x \rightarrow +\infty} \theta(x) = 0, \quad \lim_{x \rightarrow -\infty} \theta(x) = \pi. \quad (27)$$

We now turn to the proof of theorem 2. Much of the proof follows by direct analogy with the previous section. Indeed, following the proof of theorem 1, it is easy to see that lemmas 1 and 3 generalize trivially such that we can immediately restrict the admissible class to non-increasing  $\theta \in \mathcal{A}_\pi$  satisfying  $\theta(\mathbb{R}) = (0, \pi)$  along with the properties

$$\theta(0) = \frac{\pi}{2}, \quad \theta(x) = \pi - \theta(-x). \quad (28)$$

Note that we do not prove uniqueness here; the methods used to prove uniqueness for  $90^\circ$ -walls in the previous section do not apply due to the fact that the anisotropy energy is nonconvex as a function of  $u = \sin \theta$  for some values of  $\theta$  which, in this case, the profile must take. The question of uniqueness of minimizers for this problem remains open.

Lemma 2, however, does not generalize to this case. This is again due to the same issue of nonconvexity that causes problems for uniqueness. In order to obtain compactness in  $H^1(\mathbb{R})$  for the minimizing sequence, we have to prove a bound on the  $L^2(\mathbb{R})$  norm of  $\rho$ , this time defined as

$$\rho(x) = \begin{cases} \theta(x) & \text{if } \theta(x) \in [0, \pi/2], \\ \pi - \theta(x) & \text{if } \theta(x) \in [\pi/2, \pi], \end{cases} \quad (29)$$

such that once again  $\mathcal{E}_0(\theta) = \mathcal{E}_0(\rho)$ . Physically, the issue with compactness which has occurred here can be interpreted as the question of whether it is energetically preferable

for the  $180^\circ$  transition layer to split into two well-separated  $90^\circ$ -walls (which would result in the minimizing sequence weakly converging to  $\pi/2$ , which is clearly outside of the admissible class) or whether the full transition occurs mostly over a finite interval.

It is clear that the local part of the energy (25) is unchanged by having an arbitrarily large region with  $\theta = \pi/2$ . Below, we show that this is not possible due to the nonlocal term (a similar argument was used in the analysis of existence of  $360^\circ$  walls in uniaxial materials [40]). Indeed, for  $\theta$  in the above class, there exist two numbers  $0 < a < b$  such that  $\theta(a) = \pi/3$  and  $\theta(b) = \pi/6$ . From the anisotropy term alone, we get that  $b - a$  remains bounded above by a multiple of the energy. Using the known symmetry of  $\theta$  (i.e. that  $\sin \theta(-x) = \sin \theta(x)$ ), the nonlocal term in the energy (25) is proportional to

$$I = \int_0^\infty \int_0^\infty \left( \frac{(\sin \theta(x) - \sin \theta(y))^2}{(x-y)^2} + \frac{(\sin \theta(x) - \sin \theta(y))^2}{(x+y)^2} \right) dx dy. \quad (30)$$

We can estimate  $I$  from below by neglecting the interval  $(a, b)$  from the integrals. Defining

$$f(x, y) = \frac{(\sin \theta(x) - \sin \theta(y))^2}{(x-y)^2} + \frac{(\sin \theta(x) - \sin \theta(y))^2}{(x+y)^2} \geq 0, \quad (31)$$

we have

$$I \geq \int_0^a \int_0^a f(x, y) dx dy + 2 \int_0^a \int_b^\infty f(x, y) dx dy + \int_b^\infty \int_b^\infty f(x, y) dx dy. \quad (32)$$

We may then estimate the cross term as follows:

$$\int_0^a \int_b^\infty f(x, y) dx dy \geq C \int_0^a \int_b^\infty \left( \frac{1}{(x-y)^2} + \frac{1}{(x+y)^2} \right) dx dy = C \ln \left( \frac{b+a}{b-a} \right),$$

for some universal  $C > 0$ .

One can see that the nonlocal term forces both  $a$  and  $b$  to be bounded by a multiple of the energy. Then, in order to get a bound on  $\|\rho\|_{L^2(\mathbb{R})}$ , we can use the following bounds on the anisotropy energy

$$C \geq \mathcal{E}_0(\rho) \geq \frac{1}{4} \int_0^\infty \sin^2 2\theta dx = \frac{1}{4} \int_0^b \sin^2 2\theta + \frac{1}{4} \int_b^\infty \sin^2 2\theta dx. \quad (33)$$

For the second term, we have  $\theta(x) \in [0, \pi/6]$  for  $x \in [b, \infty)$ , such that  $\cos \theta \geq \sqrt{3}/2$  and  $\sin \theta \geq \theta\sqrt{3}/2$ . Using the identity  $\sin^2 2\theta = 4 \cos^2 \theta \sin^2 \theta$  we then have

$$\frac{1}{4} \int_b^\infty \sin^2 2\theta \geq \frac{9}{16} \int_b^\infty \theta^2 dx. \quad (34)$$

Additionally,

$$\int_0^b \theta^2 dx \leq C. \quad (35)$$

since we know  $b$  is finite and  $\theta(\mathbb{R}) \subset [0, \pi]$ . We can then conclude that the transition from  $\theta = \pi/2$  to  $\theta = 0$  as  $x$  increases takes place over a finite distance from  $x = 0$ , and that

$$\|\rho\|_{L^2(\mathbb{R})} \leq C, \quad (36)$$

for some  $C > 0$  depending on  $\mathcal{E}_0(\theta)$ .

One then has, for a minimizing sequence  $(\rho_n)$ , that  $\|\rho_n\|_{H^1(\mathbb{R})} \leq C$  and  $\|\sin \rho_n\|_{\dot{H}^{1/2}(\mathbb{R})} \leq C$ , for some  $C > 0$  and all  $n \in \mathbb{N}$ . One can then extract weakly convergent subsequences, and the proof of existence of minimizers, along with the regularity and strict monotonicity, follow in precisely the same fashion as in the proof of theorem 1.

## 4. Numerical study

In order to assess the role played by the one-dimensional domain wall solutions constructed in the preceding sections for the domain patterns in two-dimensional films, we use a finite-difference scheme to solve the overdamped Landau–Lifshitz–Gilbert equation (5), coupled with optimal-grid-based methods to compute the stray field. The algorithm is fully discussed in the work of MURATOV AND OSIPOV [21].

### 4.1. One-dimensional simulations

We first aim to solve (5) in 1D to obtain the wall profiles corresponding to our existence results in the previous section. We evolve the equation above, beginning from initial conditions which approximate the domain wall profile in question, until a steady state is reached. Figure 1 below displays  $90^\circ$  wall profiles for  $\nu = 1, 5$  and  $50$  (upper panels), and their corresponding tails in log-log coordinates (lower panels). Figure 2 displays the analogous plots for  $180^\circ$  walls.

Examining figures 1 and 2, one can observe that the  $90^\circ$  and  $180^\circ$  wall profiles behave in much the same manner as  $\nu$  is increased. Additionally, the tails all display algebraic decay proportional to  $1/x^2$  far from the core, as was proved to be the case for  $180^\circ$  Néel walls in uniaxial materials [30]. This decay sets in further away from the core as  $\nu$  is increased, and is clearly preceded for large  $\nu$  (e.g. in the plots for  $\nu = 50$ ) by a logarithmic crossover region between the core and the algebraic tails, as is well known for Néel walls in uniaxial materials [1, 27, 28]. We can conclude that these wall profiles show effectively the same behaviour as Néel walls in uniaxial materials. Finally, in figure 2, for  $\nu = 1$  one can see that the  $180^\circ$  wall is starting to separate into two  $90^\circ$  walls. This is due to the fact that at  $\nu = 0$  only the  $90^\circ$  walls exist, while for  $\nu > 0$  the  $180^\circ$  wall is stabilized purely by the magnetostatic interaction.

### 4.2. Two-dimensional simulations

We now solve (5) on a spatial domain  $\Omega = [0, L_x] \times [0, L_y]$  with the edges of the domain aligned with the easy axes of the material. We have effectively just three parameters in the model:  $L_x, L_y$  and  $\nu$ . Each of these has the same intuitive effect on the energy: increasing domain size or  $\nu$  increases the strength of the magnetostatic interaction, relative to anisotropy and exchange.

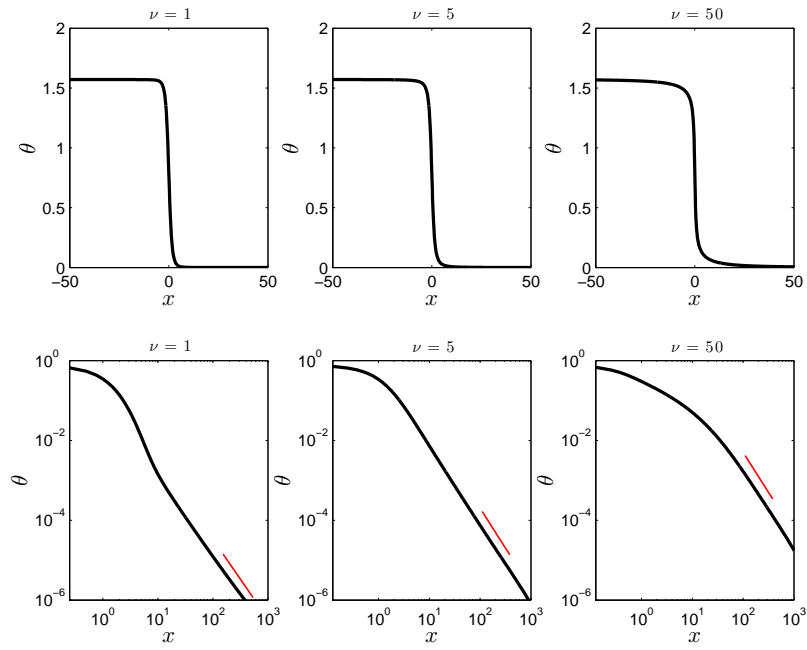


**Figure 1.** Computed 1D  $90^\circ$  wall profiles for  $\nu = 1, 5$  and  $50$ . Upper panels show the wall profiles near the transition layer. Lower panels show the corresponding decay in the tails, plotted in log-log coordinates. Red line segments in the lower panels indicate an algebraic decay of  $\theta \sim 1/x^2$ .

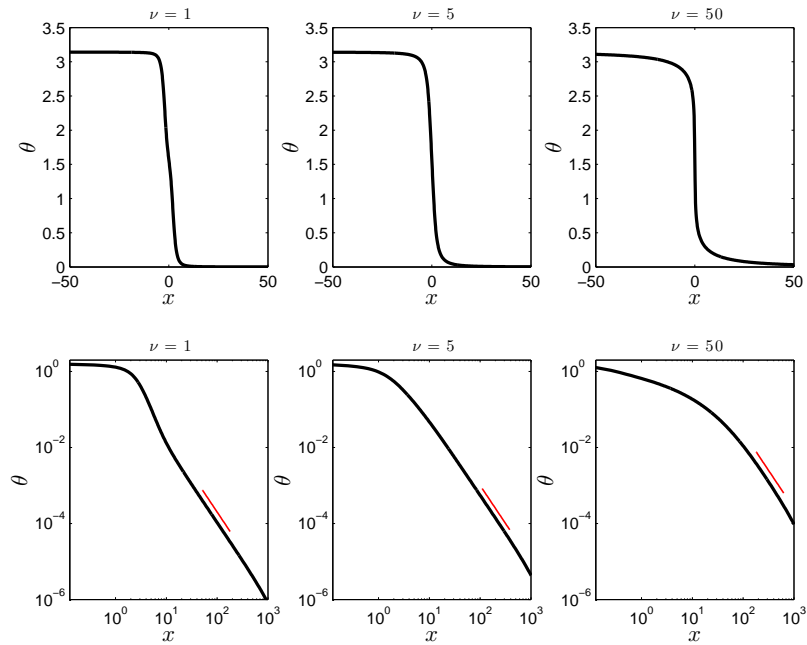


**Figure 2.** Computed 1D  $180^\circ$  wall profiles for  $\nu = 1, 5$  and  $50$ . Upper panels show the wall profiles near the transition layer. Lower panels show the corresponding decay in the tails, plotted in log-log coordinates. Red line segments in the lower panels indicate an algebraic decay of  $\theta \sim 1/x^2$ .



In the figures below we display stationary configurations (remanent states) for a range of domain sizes and values of  $\nu$ . Physically, the fixed parameters we use correspond to those of an epitaxial cobalt film, where  $\nu$  can be thought of as the suitably rescaled film thickness. The parameters (recall the definitions in equation (3)) are given approximately by  $\ell \approx 3.37\text{nm}$ ,  $Q \approx 0.08$ , and thus  $L \approx 12\text{nm}$  and  $\nu$  represents the film thickness in nanometers [22].

Starting from 3 different initial states, we can isolate 4 distinct stationary solutions, as follows. In figure 3 below we observe the well known ‘C’ (panel (a)) and ‘S’ (panel (b)) states. These states are close to monodomain states, but with edge domains appearing along the short edges of the sample to appease the magnetostatic energy at the boundary. This energy term prefers the magnetization to align tangent to the boundary wherever possible. These states result in magnetically charged regions close to the short edges, but with zero energy density in the bulk of the sample. There are necessarily half boundary vortices, which also carry charge, in two of the corners. The C state has lower energy than the S state. In both panels, the size of the sample is given (in units of  $L$ ) by  $L_x = 8, L_y = 16$  (the figures are to scale), with  $\nu = 5$ . In panel (b), the initial condition for the simulation was a monodomain with  $\theta = \pi/3$ ; in panel (a), we took  $\theta = \pi/2$  in the lower half of the sample and  $\theta = -\pi/2$  in the upper half. In the figures, the color indicates the value of  $\theta(x, y)$ , and the vectors show the corresponding magnetization field.

In figure 4, we see instead states consisting of an arrangement of  $90^\circ$  and  $180^\circ$  domain walls, with interesting phenomena appearing at the lower boundary. In both figures, one has  $L_x = 32, L_y = 64$ , and the simulations were initialized with  $\theta = 0$  in the right half of the sample and  $\theta = \pi$  in the left half. In panel (a),  $\nu = 5$ ; in panel (b),  $\nu = 10$ .

In the top halves of both panels, one observes the same phenomenology. There is a  $180^\circ$ -wall aligned vertically in the center of sample, which splits into two  $90^\circ$ -walls, which then terminate at the top corners. This arrangement separates the top half of the sample into three domains with orientations along the easy directions  $\theta = 0, \pi/2$ , and  $\pi$ , which also coincide with the orientations of the edges. The arrangements are strongly reminiscent of the so-called Landau states [1]; we refer to them as half-Landau states.

It is simple to understand why the transition from an edge-domain state to a half-Landau state is preferred as the relative strength of the magnetostatic interaction increases, just by considering the top halves of the figures. The half-Landau states are in principle charge free (in the top half), while the edge-domains are not. Thus, while sacrificing some exchange energy in order to form the domain walls, the magnetostatic energy is reduced.

In principle as mentioned above, according to the theory of section 3, each of the domain walls in the half-Landau state should be individually charge-free. While this is true of the  $180^\circ$ -wall in the center, it is not quite true of the  $90^\circ$  walls here. Indeed, their orientations are not quite at  $45^\circ$  to the easy axes, and so they are each slightly charged (in opposite senses). Since the stray-field energy of such walls would diverge

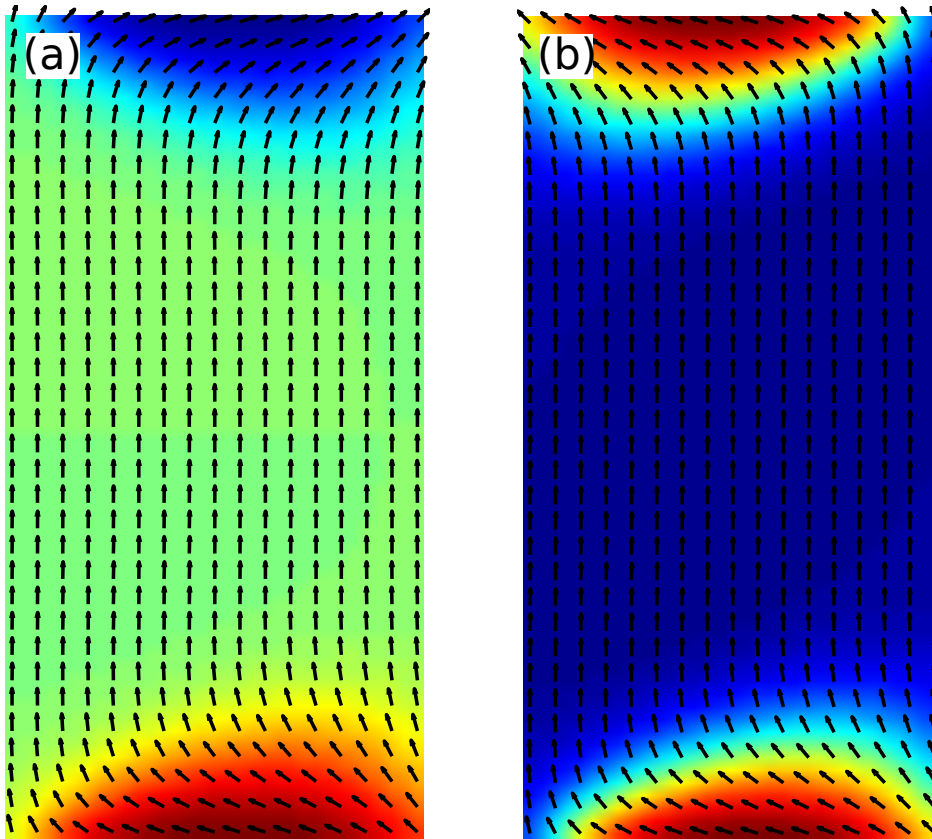


**Figure 3.** (color online) C-state (panel (a)) and S-state (panel (b)). Domain size in both panels is  $L_x = 8, L_y = 16$ , with  $\nu = 5$ .

logarithmically as the size of the domain increased, we would expect that in the large-domain limit, they would converge to a  $45^\circ$  orientation.

Let us now discuss the lower edges of the two half-Landau states pictured in figure 4. Firstly, we note that in the model we consider, the magnetization is prevented from forming the full Landau state, since in this state there would necessarily be a magnetic vortex included in the sample, and these are of infinite energy in our 2D model. Indeed, admissible magnetization states in this model must have topological degree zero (i.e. be continuously deformable to the uniform state); a vortex has degree one, as does a Landau state.

In panel (a) of figure 4, we have  $\nu = 5$ . On the lower boundary, the magnetization is aligned with  $\theta = \pi/2$ —the same as the top boundary. There are boundary vortices (quarter vortices) of opposite charges in the lower corners, and what appear to be two oppositely charged  $90^\circ$  “boundary domain walls” joining the bulk domains on the left and right to the boundary orientation. In panel (b), the magnetization on the lower boundary is instead aligned mostly with  $\theta = -\pi/2$ , antiparallel to the magnetization at top boundary, and performs a full  $2\pi$  rotation in the center of the lower edge (i.e. there is a bound pair or boundary vortices there), such that the whole configuration

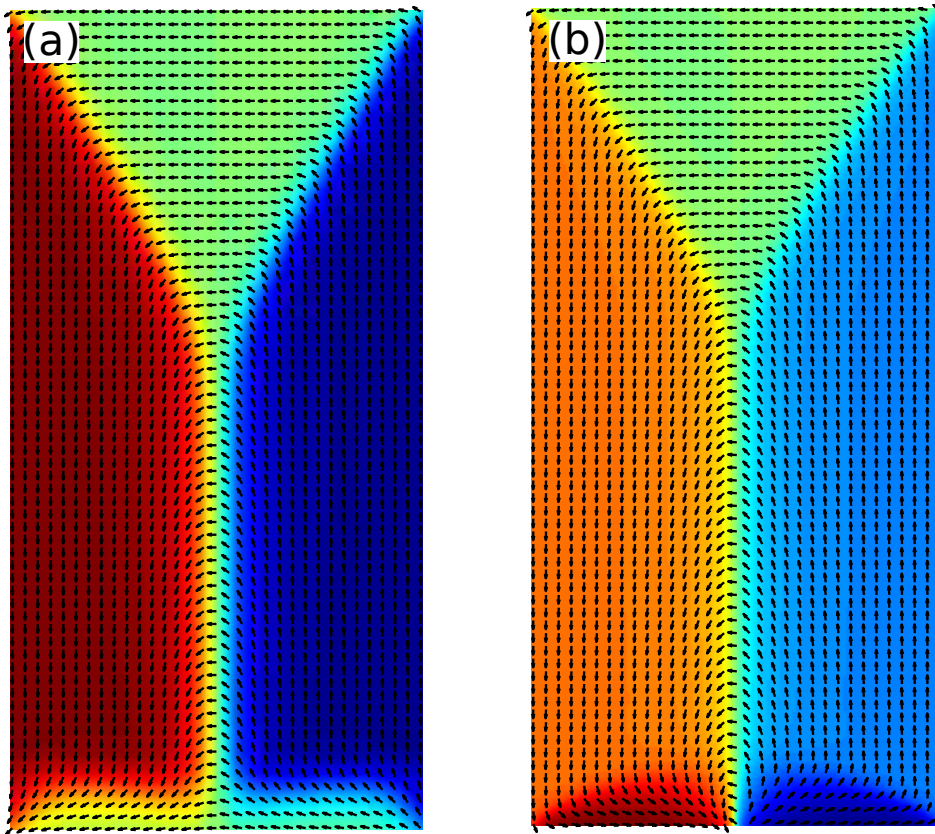


**Figure 4.** (color online) Half-Landau states. Domain size in both panels is  $L_x = 32, L_y = 64$ . In panel (a),  $\nu = 5$  and the configuration has boundary vortices in the lower corners. In panel (b),  $\nu = 10$  and we see a configuration with 2 boundary vortices as a bound pair in the center of the lower boundary.

has degree zero. Additionally, the transition layers at the lower boundary look closer in structure to edge domains than to 1D boundary walls.

In panel (a), the charge on the lower boundary is spread out across the whole edge while the exchange energy is confined close to the edge in the boundary walls. Conversely in panel (b), the charge on the boundary is focused at the bound pair of boundary vortices in the center, while the exchange energy is more spread out across the edge domains. For larger  $\nu$ , it thus appears energetically preferable to concentrate the charge in a smaller region.

## 5. Conclusions and further work

We have proven existence results concerning  $90^\circ$  and  $180^\circ$  domain walls, viewed as minimizers of the 1D domain wall energy, in thin film ferromagnets with fourfold in-plane anisotropy. Moreover we are able to learn a lot of information about these structures, including strict monotonicity, smoothness, and, in the case of  $90^\circ$ -walls, as well as uniqueness. Further problems here include proving uniqueness (or not) of the  $180^\circ$ -

wall, and studying walls with more winding such as 360°-walls, or materials with more exotic crystalline anisotropy (see, e.g., [44]). We also presented numerically computed 1D wall profiles corresponding to our existence results, and magnetization configurations for rectangular samples of fourfold materials, which feature slightly charged walls in the bulk and charged walls at the boundary. This investigation poses possible questions about domain walls in regimes where the penalty for walls having net charges is relaxed such that charged walls, both in the bulk and at the boundary may be allowed in the large domain limit, and it would be interesting to study the  $\Gamma$ -limit of such a 2D thin film energy. Additionally, there is the question of existence of ‘boundary walls’ in the thin-film regime considered in this article: this will be addressed elsewhere [45].

## Acknowledgements

This work was supported by NSF via grant DMS-1313687.

## References

- [1] A. Hubert and R. Schäfer 1998 *Magnetic Domains: The analysis of magnetic microstructures* Springer-Verlag
- [2] A. Moser *et al.* 2002 Magnetic Recording: Advancing into the Future *J. Phys. D Appl. Phys.* 35 R157–R167
- [3] Eleftheriou E, Haas R, Jelitto J, Lantz M and Pozidis H 2010 *Bulletin of the Technical Committee on Data Engineering* 33 4–13
- [4] A. DeSimone, R. V. Kohn, S. Müller, F. Otto 2000 *Magnetic microstructures—a paradigm of multiscale problems*, in: ICIAM 99 (Edinburgh), Oxford University Press, Oxford, pp. 175–190.
- [5] S. N. Piramanayagam 2007 Perpendicular recording media for hard disk drives *J. Appl. Phys.* 102 011301
- [6] C. L. Dennis, R. P. Borges, L. D. Buda, U. Ebels, J. F. Gregg, M. Hehn, E. Jouguelet, K. Ounadjela, I. Petej, I. L. Prejbeanu, and M. J. Thornton 2002 The defining length scales of mesomagnetism: a review *J. Phys. Condensed Matter* 14 R1175–R1262
- [7] J. Åkerman 2005 Toward a universal memory *Science* 308 508–510
- [8] S. Tehrani, J. M. Slaughter, M. Deherrera, B. N. Engel, N. D. Rizzo, J. Salter, M. Durlam, R. W. Dave, J. Janesky, B. Butcher, K. Smith, and G. Grynkewich 2003 Magnetoresistive random access memory using magnetic tunnel junctions *Proc. IEEE* 91 703–714
- [9] J.-G. Zhu 2008 Magnetoresistive Random Access Memory: The Path to Competitiveness and Scalability *Proc. IEEE* 96 1786–1798
- [10] R. L. Stamps *et al.* 2014 The 2014 Magnetism Roadmap *Phys. D: Appl. Phys.* 47 333001
- [11] S.D. Bader and S.S.P. Parkin 2010 Spintronics *Annu. Rev. Condens. Matter Phys.* 71–88
- [12] H. P. Oepen, M. Benning, H. Iback, C. M. Schneider and J. Kirschner 1990 Magnetic domain structure in ultrathin cobalt films *J. Magn. Magn. Mater.* 86 L137–L142
- [13] H. P. Oepen 1991 Magnetic domain structure in ultrathin cobalt films *J. Magn. Magn. Mater.* 93 116–122
- [14] G. Gioia and R. D. James 1997 Micromagnetics of very thin films *Proc. Roy. Soc. London A* 453 213–223
- [15] A. DeSimone, R. V. Kohn, S. Müller and F. Otto 2002 A reduced theory for thin film micromagnetics *Comm. Pure Appl. Math.* 55 1408–1460

- [16] R. Moser 2004 Boundary vortices for thin ferromagnetic films, *Arch. Rational Mech. Anal.* 174 267–300
- [17] M. Kurzke 2006 Boundary vortices in thin magnetic films *Calc. Var.* 26 1–28
- [18] R. V. Kohn and V. V. Slastikov 2005 Another thin-film limit of micromagnetics, *Arch. Rational Mech. Anal.* 178 227–245
- [19] B. Heinrich and J. F. Cochran 1993 Ultrathin metallic magnetic films: magnetic anisotropies and exchange interactions *Adv. Phys.* 42 523–639
- [20] C. J. Garcia-Cervera and W. E 2001 Effective dynamics for ferromagnetic thin films *J. Appl. Phys.* 90 370–374
- [21] C. B. Muratov and V. V. Osipov 2013 Optimal grid-based methods for thin film micromagnetics simulations *J. Comput. Phys.* 216 637–653
- [22] C. B. Muratov and V. V. Osipov 2009 Bit storage by 360-degree domain walls in ferromagnetic nanorings *IEEE Trans. Magn.* 45 3207–3209
- [23] C. B. Muratov, V. V. Osipov, and E. Vanden-Eijnden 2015 Energy barriers for bit-encoding states based on 360° domain walls in ultrathin ferromagnetic nanorings *J. Appl. Phys.* 117, 17D118
- [24] D. A. Allwood, G. Xiong, C. C. Faulkner, D. Atkinson, D. Petit, R. P. Cowburn 2005 Magnetic Domain-Wall Logic, *Science* 309 1688–1692
- [25] A. Aharoni 1998 *Introduction to the Theory of Ferromagnetism*, Oxford University Press, New York
- [26] C. J. Garcia-Cervera 1999 *Magnetic domains and magnetic domain walls*, PhD Thesis New York University
- [27] C. J. Garcia-Cervera 2004 One-dimensional magnetic domain walls, *Eur. J. Appl. Math.* 15 451–586
- [28] C. Melcher 2003 The logarithmic tail of Néel walls *Arch. Rational Mech. Anal.* 168 83–113
- [29] A. Capella, F. Otto and C. Melcher 2007 Wave-type dynamics in ferromagnetic thin films and the motion of Néel walls *Nonlinearity* 20 2519–2537
- [30] M. Chermisi and C. B. Muratov 2013 One-dimensional Néel walls under applied external fields *Nonlinearity* 26 2935–2950
- [31] C. B. Muratov and X. Yan 2015 Uniqueness of one-dimensional Néel wall profiles *Proc. Roy. Soc. London A* (to appear)
- [32] A. Berger and H. P. Oepen 1992 Magnetic domain walls in ultra-thin fcc cobalt films, *Phys. Rev. B* 45 12596–9
- [33] B. Y. Wong and D. E. Laughlin 1996 Direct observation of domain walls in NiFe films using high-resolution Lorentz microscopy *J. Appl. Phys.* 79 6455–7
- [34] P. O. Jubert, R. Allenspach and A. Bischof 2004 Magnetic domain walls in constrained geometries *Phys. Rev. B* 69 220410
- [35] A. DeSimone, H. Knüpfer and F. Otto 2006 2-d stability of the Néel wall *Calc. Var. Partial Differential Equations* 27 233–253
- [36] D. O. Smith and K. J. Harte 1962 Non-coherent switching in permalloy films *J. Appl. Phys.* 33 1399–1413
- [37] R. H. Wade 1964 Some factors in the easy axis magnetization of permalloy films *Philos. Mag.* 10 49–66
- [38] R. H. Wade 1965 Coercive force in thin permalloy films *Philos. Mag.* 12 437–441
- [39] C. B. Muratov and V. V. Osipov 2006 Theory of 360-degree domain walls in thin ferromagnetic films *J. Appl. Phys.* 104 053908
- [40] A. Capella-Kort, H. Knüpfer and C. B. Muratov 2015 Structure and existence of 360° Néel walls (in preparation)
- [41] Y. Jang, S. R. Bowden, M. Mascaro, J. Unguris, and C. A. Ross 2012 Formation and structure of 360 and 540 degree domain walls in thin magnetic stripes *Appl. Phys. Lett.* 100 062407
- [42] J. Zhang, S. A. Siddiqui, P. Ho, J. A. Currivan-Incorvia, L. Tryputen, E. Lage, D. C. Bono, M. A. Baldo, C. A. Ross 2015 360° Domain Walls: Stability, Magnetic Field and Electric Current Effects. <http://arxiv.org/abs/1508.07947>

- [43] E. H. Lieb and M. Loss 2010 *Analysis* American Mathematical Society
- [44] L. A. Chebotkevich, K. S. Ermakov, A. V. Ognev , E. V. Pustovalov 2011 Magnetic properties of epitaxial Co nanodisk arrays packed on atomically smooth and vicinal Si substrates *Phys. Solid State* 53 2266–2270
- [45] R. G. Lund and C. B. Muratov 2015 One-dimensional boundary domain walls in thin ferromagnetic films (in preparation)